OXYGEN NON-STOICHIOMETRY AND OXYGEN DIFFUSIVITY OF MIXED CONDUCTING PEROVSKITES

Martijn.H.R. Lankhorst, H.J.M. Bouwmeester, B.A. Boukamp and H. Verweij

University of Twente, Department of Chemical Technology,
Laboratory of Inorganic Materials Science, P.O. Box 217,
7500 AE Enschede, the Netherlands

An oxygen coulometric titration cell has been designed to measure non-stoichiometry and oxygen diffusivity of mixed oxygen ion and electronic conducting, $La_{0.8}Sr_{0.2}CoO_{3-\delta}$. Chemical diffusion data, combined with oxygen non-stoichiometry data, δ, show that the oxygen vacancy diffusion coefficient is $5.25\times e^{-(132\pm7\ kJ/mol)/RT} cm^2/s$, and independent of the oxygen partial pressure, P_{O_2}. In addition, it is found that $\log(\delta)$ is linearly related to $\log(P_{O_2})$ with slope of -0.23±0.02. The entropy associated with oxygen incorporation can be modelled with the configurational entropy of the oxygen vacancies. No electronic entropy contribution is observed. The energy of oxygen incorporation decreases almost linearly with increasing oxygen stoichiometry. Both energy and entropy data agree with a model in which electrons gradually fill electron states in a broad electron band. From the data an empirical relation between vacancy-concentration, temperature and oxygen partial pressure can be formulated, which deviates from mass action behavior.

INTRODUCTION

Cobaltite perovskite-type oxides are characterized by their large capability to accommodate deviations from oxygen stoichiometry. These materials show both high oxygen ion and electronic conductivity. As a result, non-porous membranes made from these materials can be used for separation of oxygen from air or for direct supply of oxygen into chemical reactors. Furthermore, if these oxides are used as electrode material in, for instance, solid oxygen fuel cells, oxygen sensors, pumps etc., polarization losses at the electrode can be reduced.

The aim of our ongoing research is to reveal the oxygen transport mechanism in these mixed conducting oxides. Such analysis requires both kinetic and thermodynamic studies. In an oxygen coulometric titration cell, oxygen non-stoichiometry changes and oxygen chemical diffusion coefficients can be measured simultaneously as a function of oxygen partial pressure and temperature. We have performed these measurements in order to determine the kinetic and thermodynamic properties of $La_{0.8}Sr_{0.2}CoO_{3-\delta}$.

POTENTIOSTATIC STEP METHOD

For non-stoichiometric oxides, the potentiostatic step method involves an abrupt change of the oxygen partial pressure inside a cell containing the oxide sample [1,2]. In the electrochemical cell, the oxygen partial pressure drop is induced by applying an voltage step to an oxygen ion conductor. Chemical diffusion of oxygen in the oxide sample allows the sample to change its oxygen content to a new equilibrium value. The rate of oxygen transport is measured by monitoring the electrical current through an oxygen ion conductor, required to maintain a constant oxygen partial pressure inside the cell. Equilibrium is obtained when the current has settled to a constant value equal to the leakage current. The latter value is determined by the quality of the glass seals, and the electronic conducting properties of the ionic conductors used.

In the potentiostatic mode, changes in oxygen non-stoichiometry are calculated by integrating the electric current, I, over time,

$$\Delta\delta = \frac{m_{unit\ cell}}{m_{sample}}\frac{\Delta Q}{2e} = \frac{m_{unit\ cell}}{m_{sample}}\int_{t=0}^{t=\infty}\frac{I(t)}{2e}dt \qquad (1)$$

where $m_{unit\ cell}$ and m_{sample} are the mass of the unit cell and the sample, respectively. In Eq. (1), the contribution to the total charge, ΔQ, originating from the oxygen gas inside the cell is neglected. The oxygen chemical diffusion coefficient, $\tilde{D}$, follows from the time dependence of the oxygen flux at the surface of the sample, which is directly related to the electric current. Theoretically, the transient current response to a voltage step of magnitude ΔV, is found by solving Fick's second law. In general, the solution is given in Laplace space, $I(s)$, or in Fourier space, $I(\omega)$, where ω is the angular frequency. For a disc shaped sample of thickness L and radius R, the admittance, $Y(\omega)=I(\omega)/V(\omega)$, for finite length diffusion, is found to be

$$Y(\omega)=\left(\frac{\Delta Q}{\Delta V}\right)\left(\frac{32}{\alpha\beta\tau}\right)\sum_{i\in N^*}\sum_{n\in N^*}\left(\frac{\alpha}{\alpha_i^2}+\frac{\beta}{(2n-1)^2\pi^2}\right)\left(\frac{j\omega\tau}{j\omega\tau+\frac{\alpha_i^2}{\alpha}+\frac{(2n-1)^2\pi^2}{\beta}}\right) \qquad (2)$$

where $\alpha=R^2/(R^2+L^2)$, $\beta=L^2/(R^2+L^2)$, $\tau=(R^2+L^2)/\tilde{D}$ and α_i are the zeros of the 0^{th} order Bessel function. When $R>>L$, the admittance simplifies to the well known result [3,4]

$$Y(\omega)=\left(\frac{\Delta Q}{\Delta V}\right)j\omega\sqrt{\frac{4}{j\omega\tau'}}\tanh\left(\sqrt{\frac{j\omega\tau'}{4}}\right) \qquad (3)$$

where $\tau'=L^2/\tilde{D}$. Experimentally obtained data of $I(t)$ and $V(t)$ were transformed numerically to Fourier space. From the results the admittance of the cell could be calculated, The admittance data were fitted to an equivalent circuit using the program EQUIVCRT [4]. The program was modified to incorporate an approximation of the admittance given by Eq. (2). In this manner, we were able to discriminate the influence to $I(t)$ originating from

the cell-resistance and the gas-phase capacitance from that of finite length diffusion. Details will be discussed elsewhere [5].

EXPERIMENTAL ASPECTS

Two different cell concepts were used. These are shown in fig. 1 and fig. 2. In both cells, a cylindrical disc of $La_{0.8}Sr_{0.2}CoO_{3-\delta}$ was placed in a small box with internal volume of approximately 0.26 cm^3.

In cell-1 a ZY13 ionic conducting disc was sealed to an Al_2O_3 cylindrical box using a Pyrex glass ring. Two Pt-based electrodes were painted on the inner side of the ZY13 disc using Platinum paste. These electrodes were connected to Pt wires (0.5mm) outside the cell using very thin Pt tape (0.05mm). Only one Pt-electrode was painted on the outer side of the ZY13 disc. The cell is similar to the one used by Lade and Jacobsen [6] except for the fact that our cell contains an reference electrode to account for the non-linear polarization losses at the internal $ZY/Pt/O_2$ interface, while the cell used by Lade and Jacobsen contains an reference electrode to account for the linear polarization losses at the external $ZY/Pt/O_2$ interface. However, primary experiments revealed that polarization losses at the inner electrode at low oxygen partial pressure were much larger than those at the outer electrode, that was placed in air.

Cell-2 differs from cell-1 in that the Al_2O_3 cylindrical box was replaced by a ZY13 box. In this cell arrangement, the ZY13 disc is used as oxygen sensor and the ZY13 box as oxygen pump. Pt based electrodes were painted on both sides of the disc and the box. The inner electrodes were connected to one thin Pt tape which was lead outside through the Pyrex glass ring.

$La_{0.8}Sr_{0.2}CoO_3$ powder was prepared by the EDTA synthesis [7]. After sintering, cylindrical samples were cut, 7.75 mm in diameter and 2 mm thick. The density of these samples was typically 96-98% of the theoretical one. The ZY13 discs were pressed and sintered from Zircar commercial powder.

The potentiostatic steps were applied by a Solartron 1286 electrochemical interface. A HP 7500 series B data acquisition system performed the measurements of the cell voltage and the cell current during the transient measurements. Both apparatus were controlled by computer over the IEEE parallel bus. A typical value for a potentiostatic step was 25mV. Typical values for the leakage current at 950°C are 5-20 μA for cell-1 and 15-30 μA for cell-2. At temperatures below 850°C the leakage currents were of the order of the noise. Different experiments always yielded leakage currents of the same order of magnitude. Since it can be expected that oxygen diffusion through the glass seal would lead to non-reproducible almost temperature independent leakage currents, the oxygen leak is probably due to the electronic conductivity of ZY13. Using cell-1, voltage steps were applied at 700°C, 800°C, 900°C and 1000°C between 0 and 200mV. With cell-2 similar voltage steps were applied at the temperatures: 750°C, 850°C and 950°C.

RESULTS

Oxygen diffusivity

The transformed data in most cases could be fitted fairly well to an equivalent circuit including a resistance in series with the finite length diffusion impedance given by the reciprocal of expression (2). An extra capacitance parallel to the diffusion impedance was required to fit the data at oxygen partial pressure steps near equilibrium with air. The appearance of this capacitance could be attributed to the oxygen concentration changes of the gas inside the cell. The value of the capacitance was in those cases of the same order of magnitude as the one calculated assuming the gas to behave ideally. However, the accuracy of those values was too poor in order to use the values to correct for the oxygen non-stoichiometry. A typical impedance plot is shown in fig. 3. The influence of the gas phase capacitance is seen clearly at high frequencies.

Experimentally obtained chemical diffusion coefficients are shown as a function of temperature and oxygen partial pressure in fig. 4. The results indicate that chemical diffusion coefficients obtained with cell-2 are in between the values obtained with cell-1, as they should be. The results obtained with both cells reveal that diffusion coefficients obtained from reduction steps are somewhat smaller than those obtained from oxidation steps. These differences can be attributed to the non-linear change in cell resistance during the voltage steps. The oxygen partial pressure dependence of the cell resistance could not be obtained accurately, but probably the cell resistance is mainly due to gas phase oxygen diffusion from the ZY/Pt/O_2 interface to the mixed conducting sample. Using Fick's first law and the ideal gas law, the gas phase diffusion resistance, R_{gas}, is given by

$$R_{gas} = \frac{k_B^2 T^2 L}{16 e^2 A D_{O_2} P_{O_2}} \tag{4}$$

where L is the diffusion length, A the diffusion area, k_B is Boltzmann's constant and D_{O_2} the oxygen diffusion coefficient in air. Thus one would expect the cell resistance to increase inversely proportional to the oxygen partial pressure. On the other hand, D_{O_2} is inversely proportional to the absolute pressure. This implies that gas phase oxygen diffusion would proceed much faster when no N_2 would be present in the cell. At present, the setup is modified to allow pure O_2 as reference gas.

Fig.1 shows that the chemical diffusion coefficient is almost independent of oxygen partial pressure. Theoretically one can show that for a mixed conductor with predominantly electronic conduction, the chemical diffusion coefficient is given by

$$\tilde{D} = -\frac{\sigma_O k_B T}{8 e^2 c_V} \left(\frac{d \ln P_{O_2}}{d \ln c_V}\right) = -\frac{\sigma_O k_B T}{8 e^2 c_V} \left(\frac{1}{n}\right) \tag{5}$$

where c_V is the vacancy concentration, σ_O is the oxygen ion conductivity and n is the value of the oxygen partial pressure power dependence of the vacancy concentration. As shown in the next section, n is almost constant in the oxygen partial pressure domain

where the diffusion experiments are performed. In order to relate the oxygen conductivity to the vacancy concentration, we have to make some assumptions regarding the transport process. Under the assumption that oxygen transport proceeds through an activated diffusion process over neighboring oxygen vacancies, σ_O is related to the vacancy diffusion coefficient, D_v, as follows

$$\sigma_O = \frac{D_V c_V 4e^2}{k_B T} \tag{6}$$

Combining Eq. (5) with Eq. (6) yields

$$\tilde{D} = \frac{D_V}{-2n} \tag{7}$$

where D_v is proportional to the fraction (1-δ/3). Since the latter fraction is always close to 1, the observation of a chemical diffusion coefficient almost independent of P_{O_2} is in agreement with theoretical considerations.

The activation energy for chemical diffusion can be obtained from the Arrhenius plot in fig. 5. Results obtained with both cells are plotted in the same graph. The chemical diffusion coefficients at one temperature are calculated by averaging over all diffusion coefficients at that temperature. The value for the activation energy for chemical diffusion thus obtained is equal to 132±7kJ/mol. Since the value for n is almost independent of temperature, the same activation energy is found for vacancy diffusion.

Oxygen non-stoichiometry

Oxygen stoichiometry changes can be calculated from the transient current response to a voltage step using Eq. (1). No correction was made for the change in oxygen content of the gas inside the cell. Simple calculations show that in the voltage step 0-25mV, the latter contribution to the total charge, ΔQ, is approximately 0.1C. This value cannot be neglected completely at low temperatures, since the value found for ΔQ at T=700°C is equal to 0.63C. For voltage steps at higher temperature or at lower oxygen partial pressure, neglecting the gas phase contribution is allowed. The non-stoichiometry changes were calculated as the mean value of the values obtained from the reduction and the oxidation steps. The difference between the values obtained from both steps were in all cases less than 5×10^{-4}.

In fig. 6, the results obtained with both cells are shown. The stoichiometry at T=800°C in equilibrium with air, as measured by Mizusaki [12], was taken as the reference stoichiometry. The oxygen partial pressure dependence of the non-stoichiometry was obtained from the voltage steps, while the temperature dependence was determined by measuring the open cell voltage while changing the temperature. Again the results obtained with both cells agree. If log(δ) is plotted against log(P_{O_2}), see fig. 6, straight lines are obtained with a slope equal to -0.23±0.02. The value of n, as defined in the previous section, is thus approximately equal to -0.23. The activation energy for oxygen vacancy formation is 75±15kJ/mol. The error in the activation energy is rather large due to the

non-arrhenius behavior of the oxygen non-stoichiometry. These observations are in agreement with the results obtained by Mizusaki [12].

Entropy and energy of oxygen incorporation

More insight into the solid state thermodynamics of oxygen incorporation into the perovskite lattice can be achieved by determining the entropy and energy contribution to the oxygen chemical potential [8,10]. In the electrochemical cell described above, the energy and entropy of oxygen incorporation can be obtained as follows,

$$\varepsilon_{O_2}^{bulk}=\varepsilon_{O_2}^{0}-4e\left(\frac{\partial V/T}{\partial 1/T}\right)_{I=0} \tag{8}$$

$$s_{O_2}^{bulk}=s_{O_2}^{0}+4e\left(\frac{\partial V}{\partial T}\right)_{I=0}-k_B\ln(P_{O_2}^{ref}) \tag{9}$$

where $\varepsilon_{O_2}^{0}$ and $s_{O_2}^{0}$ can be obtained from literature [9] and $P_{O_2}^{ref}$ is equal to 0.209. The condition of zero current means that no oxygen can enter or leave the cell. As a result, the oxygen stoichiometry will change only slightly due to the gas phase oxygen present in the cell. This effect can be neglected except at low temperatures and high oxygen partial pressures. The cell voltage was monitored during temperature steps of typically 25°C or 50°C. Since the results clearly indicate that energy and entropy are almost independent of temperature, it is allowed to evaluate the partial differentials in Eq. (8) and (9) by using the values of the cell voltage and temperature at the beginning and the end of a temperature step only. The results are shown in fig. 7 as a function of oxygen stoichiometry and temperature. The measurements were performed using cell-2.

The experiments reveal that ε_{O_2} can be modelled reasonably well with the following expression

$$\varepsilon_{O_2}=\varepsilon^0+\xi\times\delta \tag{10}$$

where ε^0 and ξ are approximately -290kJ/mol and -474kJ/mol, respectively. Such a dependence can be explained in terms of simple mass action type of equations only when it is assumed that the concentrations of Co^{2+} and Co^{4+} are extremely large due to *charge disproportionation*. In literature, data of oxygen non-stoichiometry [11] and of Seebeck coefficients [16] of $La_{0.8}Sr_{0.2}CoO_3$ were modelled taking into account charge disproportionation. In both cases unrealistically high concentrations of Co^{2+} and Co^{4+} species were found. However, since charge disproportionation was not observed in XAS experiments [17], it must be concluded that charge disproportionation does not take place in this oxide. The decrease in ε_{O_2} with increasing δ can also be explained if it is assumed that the *repulsive interactions between oxygen vacancies* cannot be neglected. The influence of such interactions give rise to an energy part of the oxygen vacancy chemical potential which increases linearly with increasing oxygen vacancy concentration [10]. Although the observed energy dependence can be explained perfectly in this manner, vacancy repulsion is not found in the related structure $La_{0.8}Sr_{0.2}FeO_3$ [13]. In the latter oxide, the value of the electric conduction [15] is smaller than that of $La_{0.8}Sr_{0.2}CoO_3$ [14],

and hence one expects that screening of coulombic vacancy repulsion would be even larger in the cobalt containing oxide. This implies that if oxygen vacancy interactions occur, their nature would be non-coulombic. On the other hand, both the ε_O, data and Seebeck data [16] can be explained assuming an unrealistically high degree of charge disproportionation. This implies that the physical principle underlying the observed ε_O, and Seebeck data is the same for both. Since the Seebeck coefficient does not include effects of oxygen vacancies in this material, it seems likely that the observation of a non-zero ξ does not originate from vacancy interactions. The decrease in energy with increasing non-stoichiometry can also be explained if it is assumed that the electrons formed during the creation of oxygen vacancies, gradually fill electron states of a *broad electron band*. As a result, the Fermi-energy, ε_F, gradually increases with increasing δ. This model is in agreement with the metallic like electronic conductivity in these material [14] and the observation of significant spectral intensities at the Fermi-energy with UPS [18]. Assuming the model to be correct, ξ can be related to the density of electron states at the Fermi-level, $g(\varepsilon_F)$,

$$\xi = \frac{-8}{g(\varepsilon_F)} \tag{11}$$

where $g(\varepsilon_F)d\varepsilon$ represents the number of electron states per unit cell in a small energy interval, $d\varepsilon$. The value of $g(\varepsilon_F)$ calculated using Eq. (11) turns out to be 1.6 $(eV)^{-1}$.

The obtained entropy part of the oxygen chemical potential is also shown in fig. 7. The entropy increases with increasing oxygen vacancy concentration. The observed entropy data can be fitted reasonably well with a model which includes the configurational entropy of the oxygen vacancies only.

$$s_{O_2} = -2 - s_{V_O^{\cdot\cdot}} - 4s_{e'} = s^0 - 2\,s_{V_O^{\cdot\cdot}}^{conf} = s^0 + 2\,k_B \ln\left(\frac{\delta}{3-\delta}\right) \tag{12}$$

The value of s^0 is approximately 66J/(mol×K). Apparently, the change in the electron entropy with increasing oxygen non-stoichiometry is small. Such a small electron entropy value is in agreement with the assumption of the occurrence of a broad electron band [10]. On the other hand, the agreement with the configurational entropy of the oxygen vacancies implies that the oxygen vacancies are completely disordered at the temperatures at which these measurements are performed. This was also concluded from oxygen permeation experiments [19].

From the measured energy and entropy data, the following expression can be obtained which describes the exchange reaction with gas phase oxygen

$$\left(\frac{\delta}{3-\delta}\right)^2 \left(\frac{P_{O_2}}{P_A}\right) e^{\frac{8\delta}{k_B T g(\varepsilon_F)}} = e^{\frac{-\Delta F^0}{k_B T}} \tag{13}$$

where ΔF^0 is equal to (316-0.181×T)kJ/mol. Eq. (13) differs from a mass action type of equation in that it misses the electron concentration terms, while an extra exponential term is added to account for the variable ε_O. The results shown in fig. 6 have to be in agreement with Eq. (13). This is indeed the case as will be shown below. Experimentally

it was found that at constant temperature, log(δ) changes linearly with log(P_{O_2}) with slope, n, equal to -0.23±0.02. Using the Taylor expansion near the average oxygen non-stoichiometry, <δ>

$$\delta = <\delta> + \ln(10) \times <\delta> \times \log\left(\frac{\delta}{<\delta>}\right) \tag{14}$$

it is found from Eq. (13), that for δ«3, n is given by

$$n = \frac{-1}{\left(2 + \frac{8<\delta>}{k_B T g(\varepsilon_F)}\right)}$$

Substituting the value for $g(\varepsilon_F)$, taking <δ> equal to 0.05, yields n=0.22±0.02. This value agrees with the one obtained from the potentiostatic step measurements shown in fig. 6. This example clearly shows that the potentiostatic step measurements are in agreement with the temperature step measurements. On the other hand, Eq. 15 shows that n is a measure of the density of states at the Fermi-level in these metallic like oxides.

CONCLUSIONS

Kinetic and thermodynamic parameters were determined for $La_{0.8}Sr_{0.2}CoO_{3-\delta}$ as a function of oxygen partial pressure and temperature. Under the assumption that the oxygen transport is via a simple hopping mechanism over nearest neighboring oxygen vacancies, the vacancy diffusion coefficient is found to be $5.25 \times e^{-(132\pm7\ kJ/mol)/RT} cm^2/s$, and almost independent of oxygen non-stoichiometry. The logarithm of the oxygen stoichiometry is linearly related to the logarithm of the oxygen partial pressure with slope approximately given by -0.23±0.02. The entropy associated with the incorporation of oxygen into $La_{0.8}Sr_{0.2}CoO_{3-\delta}$ is related to oxygen non-stoichiometry as can be calculated from the configurational entropy of the oxygen vacancies. No influence of the entropy of electrons was observed in the experimental data. The energy of oxygen incorporation decreases almost linearly with increasing oxygen non-stoichiometry. Both energy and entropy data can be explained with a model which assumes that electrons are placed in a broad electron band. The model implies that changes in the value of ε_{O_2} are directly related to changes in the value of the Fermi-level. An empirical expression is presented, relating oxygen non-stoichiometry to temperature and oxygen partial pressure, which clearly deviates from a mass action kind of law. This expression is in agreement with both the potentiostatic step measurements and the temperature step measurements.

REFERENCES

1 Gür, T. M., Belzner, A., Huggins, R. A., J. Membrane Sci, **75**, (1992), 151
2 Belzner, A., Gür, T. M., Huggins, R. A., Solid State Ionics, **57**, (1992), 327
3 Raistrick, I. D., Huggins, R. A., Solid State Ionics, **7**, (1982), 213
4 Boukamp, B. A., Solid State Ionics, **20**, (1986), 31
5 Boukamp, B. A., Lankhorst, M. H. R., Verweij, H., to be published
6 Lade, K., Jacobsen, T., Solid State Ionics, **72**, (1994), 218
7 Doorn, R. H. E. van, Kruidhof, H., Bouwmeester, H. J. M., Burggraaf, A. J., 'Preparation of Peovskite Ceramics by Decomposition of Metal-EDTA Complexes', submitted to J. Amer. Ceram. Soc., (1995)
8 Sørensen, O. T., 'Thermodynamics and Defect Structure of Nonstoichiometric Oxides', Nonstoichiometric Oxides, ed. Sørensen, O. T., (1981)
9 IUPAC, Commission on Thermodynamics; Oxygen , International thermodynamic tables of the fluid state-9
10 Lankhorst, M. H. R., Bouwmeester, H. J. M., Verweij, H., 'Oxidation thermodynamics and defect chemistry of late transition metal oxides', submitted to J. Amer. Ceram. Soc., (1995)
11 Hassel, B. A. van, Kawada, T., Sakai, N., Yokokawa, H., Dokiya, M., Bouwmeester, H. J. M., Solid State Ionics, **66**, (1993), 295
12 Mizusaki, J., Mima, Y., Yamauchi, S, Fueki, K., Tagawa, H., J. Sol. State. Chem., **80**, (1989), 102
13 Mizusaki, J., Yoshihiro, M., Yamauchi, S., Fueki, K., J. Sol. State Chem., **67**, (1987), 1
14 Mizusaki, J., Tabuchi, J., Matsuura, T., Yamauchi, S., Fueki, K., J. Electrochem. Soc., **136**, (1989), 2082
15 Mizusaki, J., Sasamoto, T., Cannon, W. R., Bowen, H. K., J. Amer. Cerem. Soc., **66**, (1983), 247
16 Tai, L. W., Nasrallah, M. M., Anderson, H. U., Sparlin, D. M., Sehlin, S. R., Solid State Ionics, **76**, (1995), 273
17 Abbate, M., Fuggle, J. C., Fujimori, A., Tjeng, L. H., Chen, C. T., Potze, R., Sawatzky, G. A., Eisaki, H., Uchida, S., Phys. Rev. B, **47**, (1993), 16124
18 Sarma, D. D., Chainani, A., J. Sol. State Chem., **111**, (1994), 208
19 Doorn, R. H. E. van, Kruidhof, H., Bouwmeester, H. J. M., Burggraaf, A. J., 'Oxygen permeation trough dense ceramic membranes of Sr doped $LaCoO_{3-\delta}$', submitted to J. Electrochem. Soc., (1995)

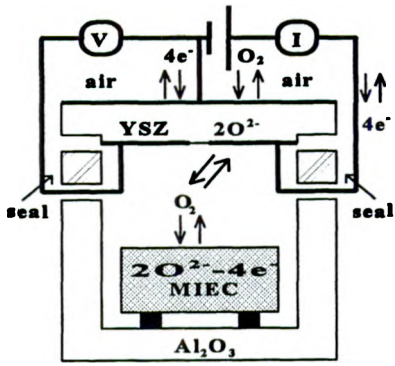

Fig. 1 Shematic plot of cell-1 used for coulometric titration experiments

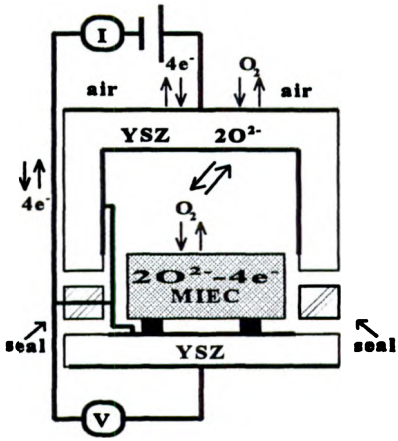

Fig. 2 Schematic plot of cell-2 used for coulometric titration experiments

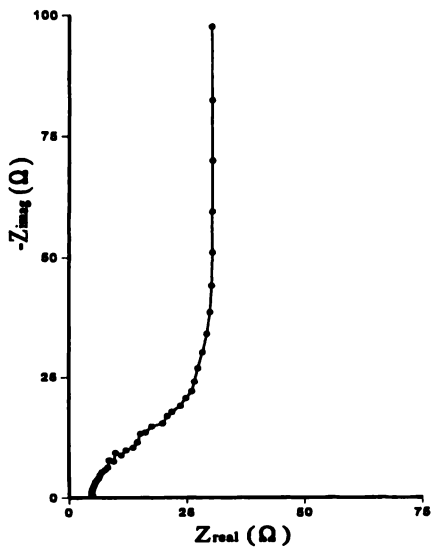

Fig. 3 Typical impedance plot including gas-phase capacitance, resistance and finite length diffusion impedance element

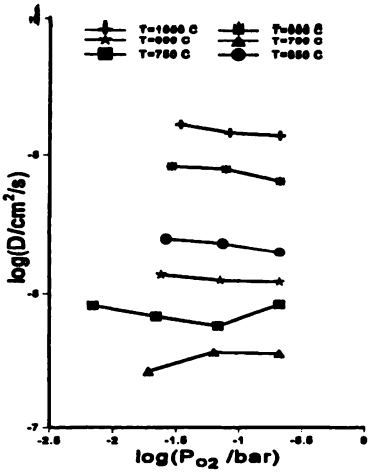

Fig. 4 Chemical diffusion in $La_{0.8}Sr_{0.2}CoO_3$ as a function of oxygen partial pressure and temperature

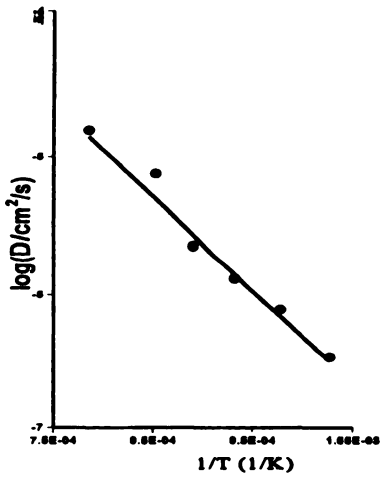

Fig. 5 Average chemical diffusion in $La_{0.8}Sr_{0.2}CoO_3$ as a function of temperature

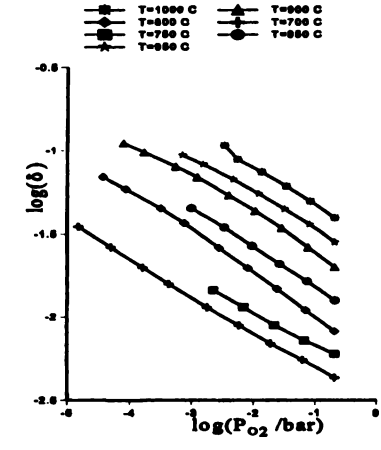

Fig. 6 Oxygen nonstoichiometry of $La_{0.8}Sr_{0.2}CoO_3$ as a function of oxygen partial pressure and temperature

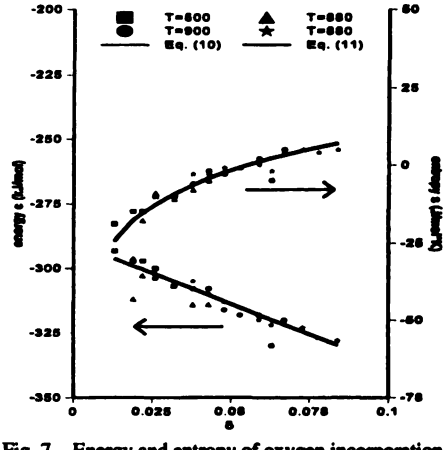

Fig. 7 Energy and entropy of oxygen incorporation in $La_{0.8}Sr_{0.2}CoO_3$ as a function of oxygen nonstoichiometry